

# Influence of geometry and loading conditions on the dynamics of martensitic fronts

Arkadi Berezovski\*

Centre for Nonlinear Studies, Institute of Cybernetics at Tallinn University of Technology,  
Akadeemia tee 21, 12618 Tallinn, Estonia

(Received June 19, 2007, Accepted October 4, 2007)

**Abstract.** Damping capacity of SMA damping devices is simulated numerically under distinct geometry and loading conditions. Two-dimensional numerical simulations are performed on the basis of a phenomenological model of dynamics of martensite-austenite phase boundaries. Results of the simulations predict the time delay and the value of the stress transferred to other parts of a construction by a damper device.

**Keywords:** shape-memory alloys; martensitic phase transformation; moving phase boundary; numerical simulation; specific damping capacity.

---

## 1. Introduction

The pseudoelastic behavior of shape memory alloys is the desired performance of dampers under seismic excitation, due to its capacity of the energy dissipation through large hysteretic cycles.

The most used shape memory alloy (SMA) in structural applications is the Nickel-Titanium alloy (Saadat, *et al.* 2002, Van Humbeeck 2003, Desroches and Smith 2004). Indeed, its pseudoelastic behavior presents several advantages, among which there are a stable hysteretic behavior, which large cycles allow the dissipation of energy, a small residual deformation, and an excellent fatigue resistance. However, a comparison analysis between Ni-Ti and Cu-based alloys is required because of a possible temperature influence.

What is important for applications of these new materials is to learn how they should be applied in a damping device.

As follows from the analysis of several earthquakes given in Marko, *et al.* (2004), a typical duration of strong motion is in the range of 1.5 - 12.5 s and dominant frequencies are in the range 0.19 - 6.39 Hz. Comparing the duration of the strong motion induced by earthquakes with the duration of the stress pulse propagation through a SMA bar, which is approximately 200  $\mu$ s, we should conclude that earthquake loads are quasistatic ones. Nevertheless, the detailed modeling of the propagation of a stress wave through a device will help to optimize the location of dampers in a structure.

In order to determine the stress wave propagation and to control corresponding displacements, we consider a constant velocity stepwise loading at the left boundary of the damper. At the right boundary we apply a non-reflective boundary condition. In an elastic material, the stepwise loading with constant

---

\*E-mail: [Arkadi.Berezovski@cs.ioc.ee](mailto:Arkadi.Berezovski@cs.ioc.ee)

velocity leads to a step-wise constant stress distribution. However, due to the martensitic transformation, we obtain a more complicated distribution of the stress inside the damper. Approximately after 200  $\mu\text{s}$ , the whole damper will be transformed into the martensitic state, and further it will be deformed elastically.

In what follows we describe the simplest possible 1-D setting of the problem of the impact-induced phase transformation front propagation in a SMA bar. Both martensitic and austenitic phases are considered as isotropic materials. The change in cross-sectional area of the bar is neglected. Since the thermal expansion coefficient of the Ni-Ti alloy is around  $6\text{--}11 \times 10^{-6} \text{ K}^{-1}$ , the thermal strain in the material is negligible under the variation up to 100 K. Therefore, the isothermal case is considered. The behavior of the material is modeled by a phenomenological approach as developed in Berezovski and Maugin (2005b).

Numerical simulations are performed in the two-dimensional case for different materials and distinct loading conditions. The main focus of the paper is on the propagation of phase-transition fronts from the impact end. The attention is paid to stress and displacement distributions in the transformation regions and to the damping capacity. Results of numerical simulations predict the time delay and the loading stress transferred to other parts of a construction by a damper device.

## 2. One-dimensional setting

We consider the boundary value problem of the tensile loading of a 1-D SMA bar that is initially in an austenitic phase and that has uniform cross-sectional area  $A_0$  and temperature  $\theta_0$ . The bar occupies the interval  $0 < x < L$  in a reference configuration and the boundary  $x = 0$  is subjected to the tensile shock loading

$$\sigma(0, t) = \hat{\sigma}(t) \quad \text{for } t > 0 \quad (1)$$

The bar is assumed to be long compared to its diameter so it is under uni-axial stress state and the stress  $\sigma(x, t)$  depends only on the axial position and time. Supposing the temperature is constant during the process, it is characterized by the displacement field  $u(x, t)$ , where  $x$  denotes the location of a particle in the reference configuration and  $t$  is time. Linearized strain is further assumed so the axial component of the strain  $\varepsilon(x, t)$  and the particle velocity  $v(x, t)$  are related to the displacement by

$$\varepsilon = \frac{\partial u}{\partial x}, \quad v = \frac{\partial u}{\partial t} \quad (2)$$

The density of the material  $\rho$  is assumed constant. All field variables are averaged over the cross-section of the bar.

At each instant  $t$  during a process, the strain  $\varepsilon(x, t)$  varies smoothly within the bar except at phase boundaries; across a phase boundary, it suffers jump discontinuity. The displacement field is assumed to remain continuous throughout the bar. Away from a phase boundary, the balance of linear momentum and the kinematic compatibility require that

$$\rho \frac{\partial v}{\partial t} = \frac{\partial \sigma}{\partial x} \quad (3)$$

$$\frac{\partial \varepsilon}{\partial t} = \frac{\partial v}{\partial x} \quad (4)$$

Suppose that at time  $t$  there is a moving discontinuity in strain or particle velocity at  $x = S(t)$ . Then one

also has the corresponding jump conditions

$$\rho V_S [v] + [\sigma] = 0 \quad (5)$$

$$V_S [\varepsilon] + [v] = 0 \quad (6)$$

where  $V_S$  is the velocity of the moving phase boundary and square brackets denote jumps, i.e.,  $[A] = A^+ - A^-$ .

The second law of thermodynamics requires that

$$f_S V_S \geq 0 \quad (7)$$

at strain discontinuities. Here the driving force  $f_S(t)$  at the discontinuity is defined by Truskinovsky (1987)

$$f_S = -[W] + \langle \sigma \rangle [\varepsilon] \quad (8)$$

where  $W$  is the free energy per unit volume and  $\langle \sigma \rangle = (\sigma^+ + \sigma^-)/2$ .

If  $f_S$  is not zero, the sign of  $V_S$ , and hence the direction of motion of discontinuity, is determined by the sign of  $f_S$ .

The difficulties in solution are related to an unknown motion of the phase boundary and to the jump relations across it.

### 2.1. Numerical scheme

The formulated uniaxial dynamic problem (3)-(4) can be solved by means of the finite-volume numerical scheme (Berezovski and Maugin 2001), which is reduced in the considered case to

$$(\bar{v})_n^{l+1} - (\bar{v})_n^l = \frac{\Delta t}{\Delta x \rho_n} ((\Sigma^+)_n^l - (\Sigma^-)_n^l) \quad (9)$$

$$(\bar{\varepsilon})_n^{l+1} - (\bar{\varepsilon})_n^l = \frac{\Delta t}{\Delta x} ((\mathcal{V}^+)_n^l - (\mathcal{V}^-)_n^l) \quad (10)$$

Here subscript denotes number of computational cell and superscript denotes time step.

What we need is to determine the values of excess quantities  $\Sigma$  and  $\mathcal{V}$  and the velocity of the phase boundary.

#### 2.1.1. Excess quantities in the bulk

In the admitted non-equilibrium description (Muschik and Berezovski 2004), both stress and velocity are represented as the sum of averaged (local equilibrium) and excess parts:

$$\sigma = \bar{\sigma} + \Sigma, \quad v = \bar{v} + \mathcal{V} \quad (11)$$

Here  $\bar{\sigma}$  and  $\bar{v}$  are averaged fields and  $\Sigma$  and  $\mathcal{V}$  are the corresponding excess quantities.

In the isothermal case, we require that the total stress should be continuous across the boundary between cells

$$[\bar{\sigma} + \Sigma] = 0 \quad (12)$$

This means that at the interface between elements  $(n-1)$  and  $(n)$  in the uniaxial case we have

$$(\Sigma^+)_{n-1} - (\Sigma^-)_n = (\bar{\sigma})_n - (\bar{\sigma})_{n-1} \quad (13)$$

Therefore, the jump relation (12) can be considered as the *continuity of genuine unknown field* at the boundaries between computational cells.

The jump relation following from the kinematic compatibility (6) reads

$$[\bar{v} + \mathcal{V}] = 0 \quad (14)$$

Therefore, in the uniaxial case

$$(\mathcal{V}^+)_{n-1} - (\mathcal{V}^-)_n = (\bar{v})_n - (\bar{v})_{n-1} \quad (15)$$

Using the conservation of “Riemann invariants” for excess quantities (Berezovski and Maugin 2005b)

$$(\Sigma^-)_n + \rho_n c_n (\mathcal{V}^-)_n = 0 \quad (16)$$

$$(\Sigma^+)_{n-1} - \rho_{n-1} c_{n-1} (\mathcal{V}^+)_{n-1} = 0 \quad (17)$$

we obtain then the system of linear equations for the determination of excess quantities. This system of equations can be solved exactly for each boundary between computational cells. After that the field quantities can be updated for the next time step by means of the numerical scheme (9)-(10).

### 2.1.2. Excess quantities at the phase boundary

To determine the values of excess stresses at the moving phase boundary, we keep the continuity of excess stresses across the phase boundary (Berezovski and Maugin 2005b)

$$[\Sigma] = 0 \quad (18)$$

which yields

$$(\Sigma^+)_{p-1} - (\Sigma^-)_p = 0 \quad (19)$$

where phase boundary is placed between elements  $(p-1)$  and  $(p)$ .

The last jump relation can be interpreted as the *conservation of the genuine jump at the phase boundary* in the numerical calculations because Eq. (18) means that

$$[\sigma] = [\bar{\sigma} + \Sigma] = [\bar{\sigma}] \quad (20)$$

To be consistent, we require the conservation of the genuine jump also for velocity

$$[\mathcal{V}] = 0 \quad (21)$$

We still keep the relations between excess stresses and excess velocities (16), (17). This means that in terms of excess stresses Eq. (21) yields

$$\frac{(\Sigma^+)_{p-1}}{\rho_{p-1} c_{p-1}} + \frac{(\Sigma^-)_p}{\rho_p c_p} = 0 \quad (22)$$

It follows from the conditions (19) and (22) that the values of excess stresses vanish at the phase boundary

$$(\Sigma^+)_{p-1} = (\Sigma^-)_p = 0 \quad (23)$$

Now all the excess quantities at the phase boundary are determined, and we can update the state of the

elements adjacent to the phase boundary.

However, the proposed procedure should be applied at the phase boundary only after the initiation of the phase transition process. The possible motion of the interface between phases should also be taken into account.

## 2.2. Velocity of the phase boundary

The velocity of the phase boundary can be calculated by means of the jump relation corresponding to the balance of linear momentum which can be represented in a one-dimensional case as

$$V_s[\rho_0 v] + [\rho] = 0 \quad (24)$$

The only difficulty is that all fields should be determined in advance, accounting the unknown velocity of the front.

At the phase boundary we apply the continuity of excess quantities (Berezovski and Maugin 2005b)

$$[\Sigma] = 0, \quad [\mathcal{V}] = 0 \quad (25)$$

which leads to the jump relation for linear momentum in terms of averaged quantities

$$V_s[\rho_0 \bar{v}] + [\bar{\sigma}] = 0 \quad (26)$$

and simultaneously determines the value of the jump of the averaged stress at the phase boundary for a thermoelastic body (Berezovski and Maugin 2005a)

$$[\bar{\sigma}] = -2\theta_0 [\alpha(3\lambda + 2\mu)] \quad (27)$$

Here  $\theta_0$  is the reference temperature,  $\alpha$  is the coefficient of thermal expansion,  $\lambda$  and  $\mu$  are Lamé coefficients.

Having the value of the stress jump, we can derive the relation for the determination of the velocity of the front in terms of the stress jump (Berezovski and Maugin 2005b)

$$\rho_0 V_s^2 = \frac{[\bar{\sigma}]}{A[\bar{\sigma}] - B} \quad (28)$$

or in terms of the driving force

$$\rho_0 V_s^2 = \frac{f_s}{Af_s - B/D} \quad (29)$$

because the stress jump and the driving force are related (in the isothermal case) as follows (Berezovski and Maugin 2005b).

$$f_s \left[ \frac{1}{\alpha(3\lambda + 2\mu)} \right] = \frac{\theta_0 [\bar{\sigma}]}{2} \left[ \frac{1}{\lambda + 2\mu} \right] \quad (30)$$

Here  $f_s$  is the driving force,  $A$ ,  $B$  and  $D$  are coefficients depending on material properties and transformation strain. Eq. (30) is nothing else but the kinetic relation for the phase transition front propagation.

### 3. Numerical procedure

Numerical solution of the system of Eqs. (3)-(4), complemented by equation of state and extended to the two-dimensional case, is obtained by means of the numerical scheme described in previous sections. This is the explicit high-order accurate wave propagation algorithm (LeVeque 1997) specifically adopted for the case of moving discontinuities (Berezovski and Maugin 2005b). A procedure similar to a cellular automaton is applied to the phase-transition front tracking. At any time step, the values of the driving force are calculated in cells adjacent to the phase boundary. If the value of the driving force at the phase boundary exceeds the critical one, the velocities of the phase front are computed. Virtual displacements of the phase-transition front are calculated then for all possible phase boundaries adjacent to the cell. We keep the cell in the old phase state if the (algebraic) sum of the virtual displacements is less than the size of space step, and change it to another phase otherwise. All the calculations are performed with the Courant-Friedrichs-Levy number equal to 1.

### 4. Results of simulation

First, we consider a constant velocity step-wise loading at the left boundary of the damper, as it is shown in Fig. 1. At the right boundary we apply a non-reflective boundary condition. The amplitude of the loading was chosen to overcome the critical value of the driving force.

#### 4.1. Material properties

Calculations are performed for three different shape memory alloys listed in Table 1. The corresponding mechanical properties are given in Table 2.



Fig. 1 Geometry of the test problem

Table 1 Shape memory alloys

Alloy composition	Source
Ni-Ti(50 wt. %)	McKelvey and Ritchie (2000)
Cu-Zn(25.63 wt.%)-Al(4.2 wt.%)	Goo and Lexcelent (1997)
Cu-Al(11.8 wt.%)-Be(0.5 wt.%)	Casciati, <i>et al.</i> (2007)

Table 2 Material properties

	Ni-Ti	Cu-Zn-Al	Cu-Al-Be
Density (kg/m <sup>3</sup> )	6450	8228	8500
Young modulus - austenite (GPa)	62	67.25	60
Young modulus - martensite (GPa)	22	32	30
Poisson's ratio	0.33	0.33	0.3

### 4.2. Displacement at left and right ends

We will compare the displacements at left and right ends of the damper under different loading conditions and for various shape-memory alloys.

#### 4.2.1. Plane wave conditions

We start with plane wave conditions. These conditions fully correspond to the one-dimensional setting. It is clear that in the absence of martensitic phase transformation, displacements at both ends should be similar. It is illustrated in Fig. 2, where calculations are performed for the pure austenitic Ni-Ti alloy. Here we observe no damping, but only a time delay in the displacement history.

The situation is changed, if the martensitic phase transformation occurs. Fig. 3 represents the time history of displacement in the case of one-dimensional martensitic front propagation in SMA dampers under plane wave conditions.

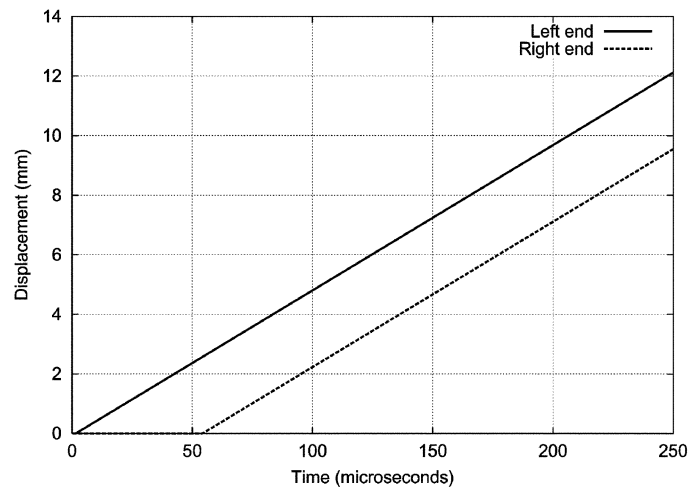


Fig. 2 Time history of displacements. No phase transformation

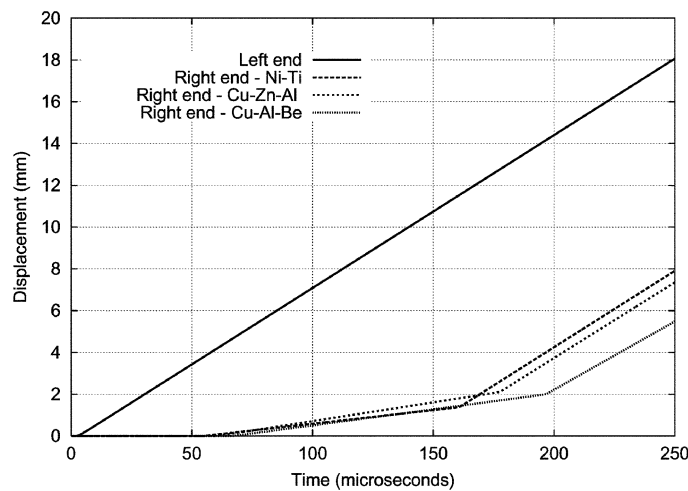


Fig. 3 Time history of displacements. One-dimensional front propagation in SMA dampers



Fig. 4 Non-plane wave loading

All three SMAs demonstrate the difference from the previous case (with no phase transformation) in the displacements history due to the martensitic phase transition front propagation. The elastic regime at the right end for Ni-Ti alloy starts at  $\sim 160 \mu\text{s}$ , when the damper is fully transformed. A similar behaviour is observed for the Cu-Zn-Al SMA. However, the displacement at the right end for Cu-Zn-Al SMA returns to the elastic regime at  $180 \mu\text{s}$ , but the value of the displacement at this point is slightly bigger than in the case of the Ni-Ti SMA. For the Cu-Al-Be damper, the displacement at the right end is first almost the same as for the Ni-Ti damper, but the phase transformation is finished later than in previous cases.

#### 4.2.2. Non-plane wave conditions

Now we change the loading conditions at the left end to the two-dimensional case (Fig. 4). We apply the constant velocity step-wise loading only at a part of the left boundary, upper and bottom boundaries are stress free. The geometry of the damper remains unchanged. The results of calculations are given in Fig. 5.

As one can see, the displacement history at the right end of the damper is more smooth than in the case of plane wave conditions, and the elastic regime starts only at  $\sim 225 \mu\text{s}$ . This related to the delay with the full martensitic transformation of the damper due to the two-dimensional front propagation.

The overall behavior of the displacement at the right end for the Cu-Zn-Al SMA is very similar to the case of the Ni-Ti SMA, but the values of the displacement are slightly larger. As previously, the most low values of the displacement at the right end is demonstrated by the Cu-Al-Be SMA.

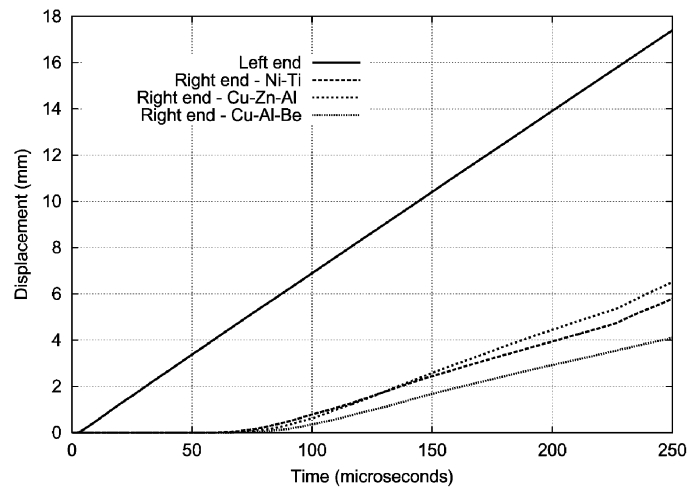


Fig. 5 Time history of displacements. Two-dimensional front propagation in SMA dampers

#### 4.2.3. Stress distribution and front location

Snapshots of wavefronts and the corresponding location of the phase boundary at different time instants are shown in Fig. 6 on the example of Cu-Zn-Al damper. As one can see, the propagation of stress waves, their reflections from upper and bottom boundaries and the interaction with the moving phase transition front form the shape of the front itself. This shows clearly how the loading conditions affect the propagation of the phase transition front in the two-dimensional case.

#### 4.3. Damper with a hole

Now we analyze another shape of the damper as well as loading conditions. We consider a damper with a hole, which may be used for the connection to other parts of a construction. The constant velocity step-wise loading is also applied at the hole. Left, upper, and bottom boundaries are stress free. The non-reflective boundary condition remains at the right boundary. The geometry of the problem is shown in Fig. 7.

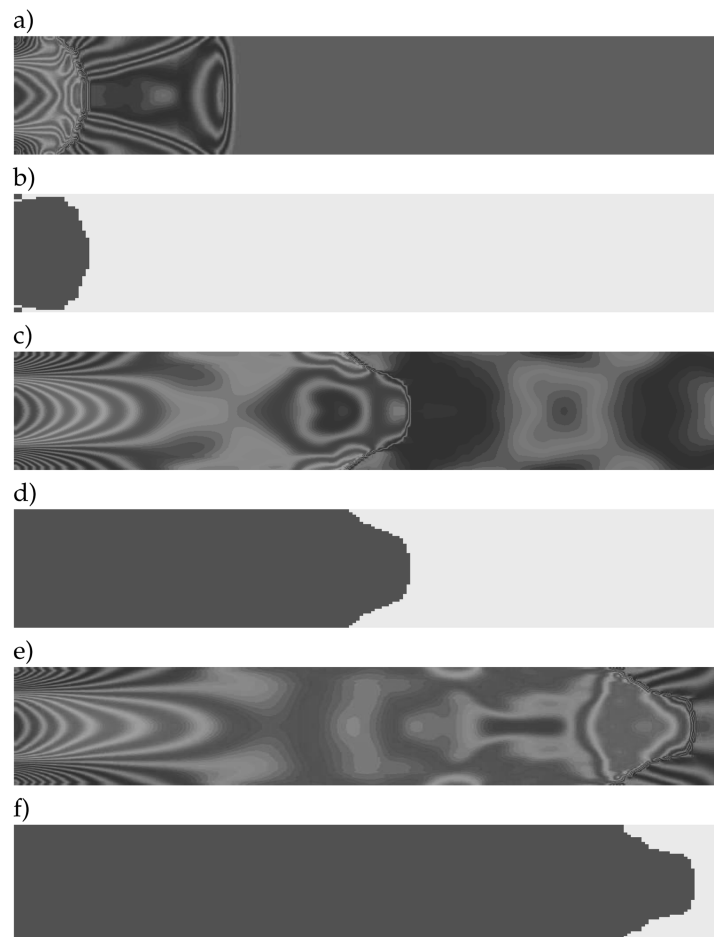
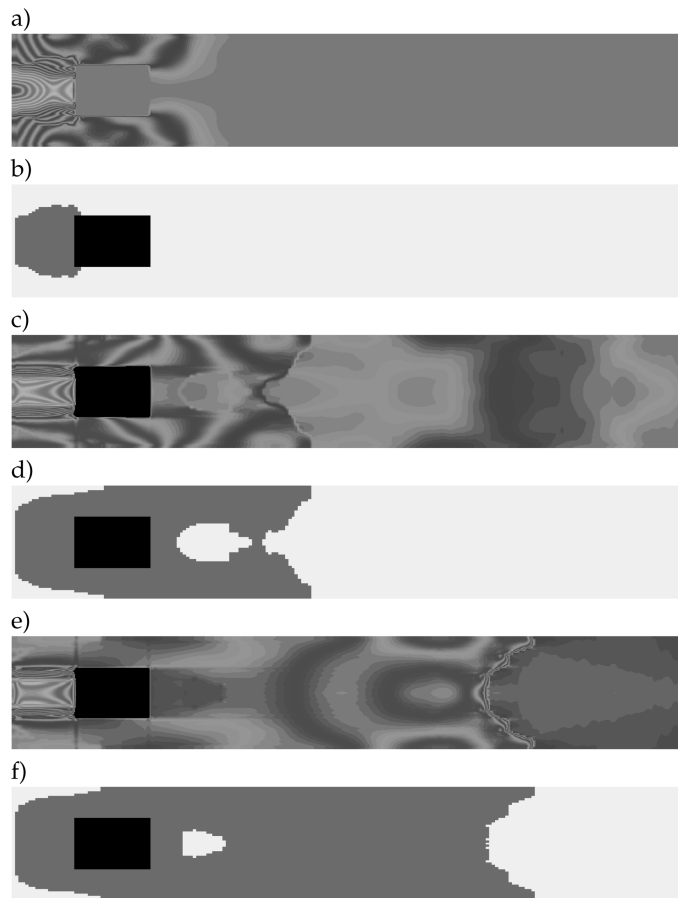


Fig. 6 Snapshots of wave distribution and front propagation in Cu-Zn-Al SMA damper: a) wave distribution, b) front location at 20  $\mu\text{s}$ , c),d) -at 120  $\mu\text{s}$ , e),f) -at 220  $\mu\text{s}$ .



Fig. 7 Test problem for a damper with a hole

Fig. 8 Snapshots of wave distribution and front propagation in Ni-Ti SMA damper with a hole: a) wave distribution, b) front location at 20  $\mu\text{s}$ , c),d) -at 120  $\mu\text{s}$ , e),f) -at 220  $\mu\text{s}$ 

#### 4.3.1. Stress distribution and front location

Snapshots of the stress wave propagation and the corresponding location of the phase boundary are shown in Fig. 8 on the example of the Ni-Ti SMA.

As we can see, the stress is concentrated between the hole and the left boundary of the damper, which is an expected result.

The corresponding displacement history for the Ni-Ti and Cu-Zn-Al SMAs is presented in Fig. 9. Here we can observe an extremely low displacement at the right end both for the Ni-Ti and Cu-Zn-Al SMAs due to the changed loading conditions.

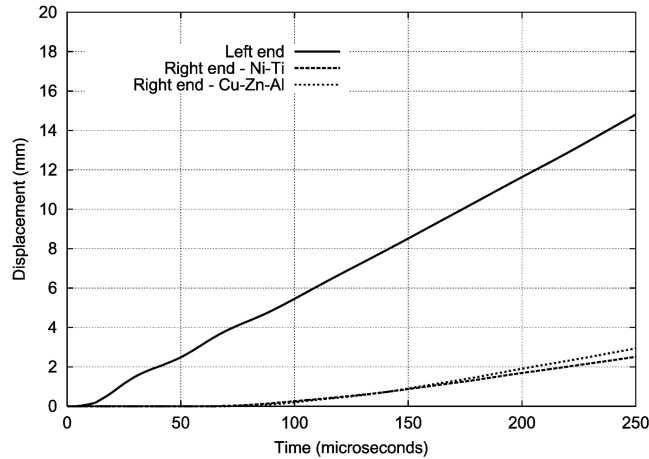


Fig. 9 Time history of displacements for Ni-Ti and Cu-Zn-Al dampers with a hole

It looks like that dampers with a hole are more efficient for applications in constructions than dampers without the hole. However, there is another important characteristic for the damping: energy dissipation.

## 5. Energy dissipation

It is well known (Abeyaratne and Knowles 2006) that the movement of the austenite-martensite phase boundary acts as an active mechanism for the conversion of mechanical to thermal energy. The rate of energy dissipated by the moving discontinuity in the one-dimensional case is given by

$$D = \int f_S V_S dA \quad (31)$$

where  $A$  is the surface of the front. Integrating the above expression over the front surface and over time, we can determine the specific damping capacity, comparing the dissipation of the energy with the the maximum stored elastic energy (Van Humbeeck and Kustov 2005). The results of calculations of the dimensionless specic damping capacity for the Ni-Ti dampers are shown in Fig. 10. Here we can see the opposite tendency: the damper with a hole has much lower damping capacity than the dampers without the hole.

As regards to different materials, we have compared first the specific damping capacity for dampers made from the Ni-Ti and from the Cu-Zn-Al SMAs. The result of the comparison is presented in Fig. 11 in the case of non-plane wave loading. As one can see, the damping capacity for the Ni-Ti SMA is higher that those for the Cu-Zn-Al SMA. The calculated value of the specific damping capacity for the Cu-Zn-Al damper corresponds to the experimentally observed value (Van Humbeeck and Kustov 2005).

It should be noted that the specific damping capacity for the Cu-Al-Be damper under plane wave conditions (Fig. 12) is higher than for the Ni-Ti damper. Just this material is proposed for the retrofitting of historical monuments.

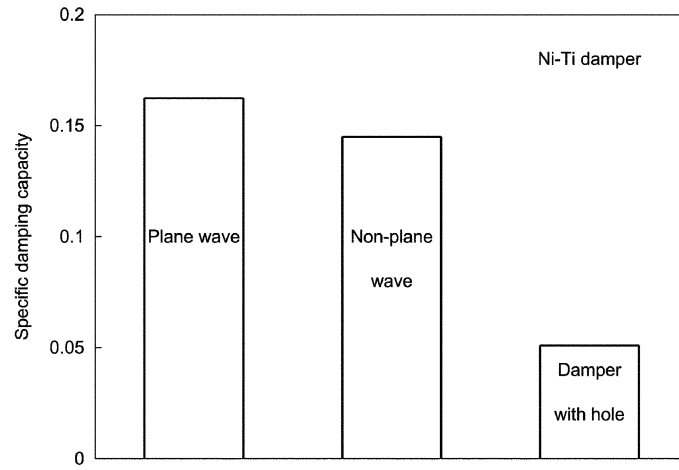


Fig. 10 Specific damping capacity for Ni-Ti dampers

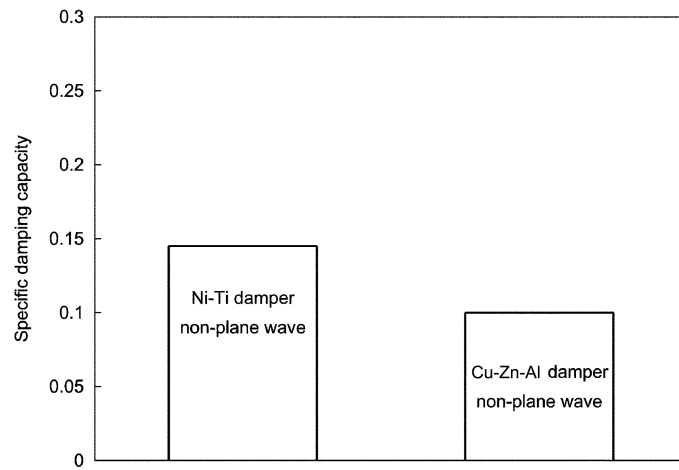


Fig. 11 Specific damping capacity for Ni-Ti and Cu-Zn-Al dampers

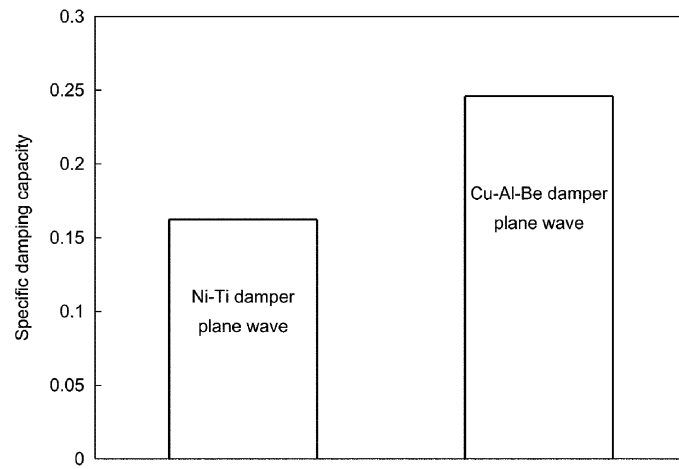


Fig. 12 Specific damping capacity for Ni-Ti and Cu-Al-Be dampers

## 6. Conclusions

Numerical simulations of martensitic phase-transition front propagation in two-dimensional case show that the damping capacity of SMA damping devices depends essentially on geometry and loading conditions.

As we have seen, this dependence is not simple. If we pay attention only for loading conditions, the geometry of damper with a hole looks like preferred. However, the energy dissipation is more efficient for dampers with simple geometry.

Additionally, it is shown that the damping capacity is also material depending.

## Acknowledgment

Support of the Estonian Science Foundation and the European Community under contract INCO-CT-2004-509085 is gratefully acknowledged.

## References

- Abeyaratne, R. and Knowles, J. K. (2006), *Evolution of Phase Transitions: A Continuum Theory*, Cambridge University Press, Cambridge, UK.
- Berezovski, A. and Maugin, G. A. (2001), "Simulation of thermoelastic wave propagation by means of a composite wave-propagation algorithm", *J. Comput. Physics*, **168**, 249-264.
- Berezovski, A. and Maugin, G. A. (2005a), "On the velocity of a moving phase boundary in solids", *Acta Mech.*, **179**, 187-196.
- Berezovski, A. and Maugin, G. A. (2005b), "Stress-induced phase-transition front propagation in thermoelastic solids", *Eur. J. Mech. -A/Solids*, **24**, 1-21.
- Casciati, F., Casciati, S. and Faravelli, L. (2007), "Fatigue characterization of a Cu-based shape memory alloy", *Proc. Estonian Acad. Sci. Phys. Math.*, **56**, 207-217.
- Desroches, R. and Smith, B. (2004), "Shape memory alloys in seismic resistant design and retrofit: a critical review of their potential and limitations", *J. Earthq. Eng.*, **8**, 415-429.
- Goo, B. C. and LExcellent, C. (1997), "Micromechanics-based modeling of two-way memory effect of a single-crystalline shape-memory alloy", *Acta Mater.*, **45**, 727-737.
- LeVeque, R.J. (1997), "Wave propagation algorithms for multidimensional hyperbolic systems", *J. Comput. Physics*, **131**, 327-353.
- Marko, J., Thambiratnam, D. and Perera, N. (2004), "Influence of damping systems on building structures subject to seismic effects", *Eng. Struct.*, **26**, 1939-1956.
- McKelvey, A. L. and Ritchie, R. O. (2000), "On the temperature dependence of the superelastic strength and the prediction of the theoretical uniaxial transformation strain in Nitinol", *Phil. Mag. A*, **80**, 1759-1768.
- Muschik, W. and Berezovski, A. (2004), "Thermodynamic interaction between two discrete systems in non-equilibrium", *J. Non-Equilibrium Thermodyn.*, **29**, 237-255.
- Saadat, S., Salichs, J., Noori, M., Hou, Z., Davoodi, H., Baron, I., Suzuki, Y. and Masuda, A. (2002), "An overview of vibration and seismic applications of NiTi shape memory alloy", *Smart Mater. Struct.*, **11**, 218-229.
- Truskinovsky, L. (1987), "Dynamics of nonequilibrium phase boundaries in a heat conducting nonlinear elastic medium", *J. Appl. Math. Mech. (PMM)*, **51**, 777-784.
- Van Humbeeck, J. (2003), "Damping capacity of thermoelastic martensite in shape memory alloys", *J. Alloys Compounds*, **355**, 58-64.
- Van Humbeeck, J. and Kustov, S. (2005), "Active and passive damping of noise and vibrations through shape memory alloys: applications and mechanisms", *Smart Mater. Struct.*, **14**, S171-S185.